ACS OMEGA

http://pubs.acs.org/journal/acsodf

Article

Optimization of an Antibody Microarray Printing Process Using a Designed Experiment

Alexander J. Summers,* Jasmine P. Devadhasan, Jian Gu,* Douglas C. Montgomery,* Brittany Fischer, Marcellene A. Gates-Hollingsworth, Kathryn J. Pflughoeft, Tuan Vo-Dinh, David P. AuCoin, and Frederic Zenhausern*

Cite This: *ACS Omega* 2022, 7, 32262−32271

Read Online

ACCESS | Metrics & More | Article Recommendations | Supporting Information

ABSTRACT: Antibody microarrays have proven useful in immunoassay-based point-of-care diagnostics for infectious diseases. Noncontact piezoelectric inkjet printing has advantages to print antibody microarrays on nitrocellulose substrates for this application due to its compatibility with sensitive solutions and substrates, simple droplet control, and potential for high-capacity printing. However, there remain real-world challenges in printing such microarrays, which motivated this study. The effects of three concentrations of capture antibody (cAb) reagents and nozzle hydrostatic pressures were chosen to investigate three responses: the number of printed membrane disks, dispensing performance, and microarray quality. Printing conditions were found to be most ideal with 5 mg/mL cAb and a nozzle hydrostatic pressure near zero, which produced 130 membrane disks in a single print versus the 10 membrane disks per print before optimization. These results serve to inform efficient printing of antibody microarrays on nitrocellulose membranes for rapid immunoassay-based detection of infectious diseases and beyond.

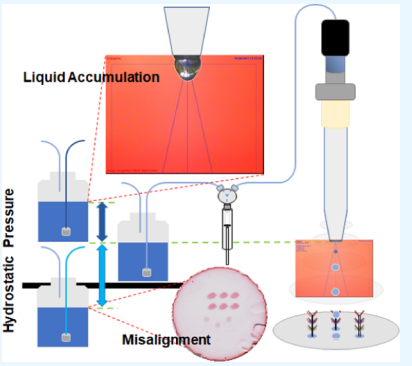

1. INTRODUCTION

Antibody microarrays are currently being used for numerous applications including analysis of proteins, nucleic acids, cell surface proteins, and simultaneous detection of these analytes.[1−7] They have contributed significantly to "life-omics", as well as disease diagnostics and management.[8] In general, antibody arrays are fabricated by immobilizing multiple antibodies on a solid substrate, such as a chemically treated glass slide or well plate, or a nitrocellulose (NC) paper membrane, to analyze antibody−antigen interactions.[9] Due to the assay cost associated with a large number of antibodies, microarray fabrication emerged to miniaturize the arrays with thousands of spots within centimeters.

Different technologies have been utilized to print antibody arrays, including contact printing (pin, stamp, stencil, and microfluidic printings), noncontact printing (inkjet printing), lithography printing (photolithography, electron beam lithography), and atomic force microscopy (AFM) printing (dip-pen lithography and nanoshaving).[8] Each printing technology has their own merits and drawbacks. However, current commercial microarray printing systems mainly focus on two printing technologies, i.e., pin contact printing and inkjet noncontact printing.[10] Though pin contact printing can offer the capability of dispensing high-viscosity samples and ease of control, this method is prone to damaging the substrate, with lower protein activity, poor precision, and low work efficiency.[11−13] On the other hand, noncontact inkjet printing is advantageous for printing on NC membranes without damaging the substrate, which is the main application of this paper.[14]

Inkjet printing can be classified as continuous inkjet (CIJ) and drop-on-demand (DOD) printings by mechanism or thermal and piezoelectric inkjet printings by actuation.[15] For printing functional materials, DOD piezoelectric inkjet printing is mostly used because of the economical ink usage of DOD printing and flexibility of changing the actuation pulse to control drop size and velocity for any fluid by piezoelectric printing.[15] Although used commercially, there are still problems reported for DOD piezoelectric inkjet printing, such as failure of droplet formation, inaccurate droplet placement etc., which were also observed in our experiments.[16]

Droplet formation, control, and jet straightness are complex processes affected by multiple parameters, such as fluid properties of the ink, printhead design, wetting, and bubbling at the nozzle etc.[17] It is even more complicated to print complex fluids such as an antibody solution because a change of a single solution parameter (such as the antibody concentration) can affect multiple printing properties (such

Received: June 8, 2022
Accepted: August 15, 2022
Published: August 30, 2022

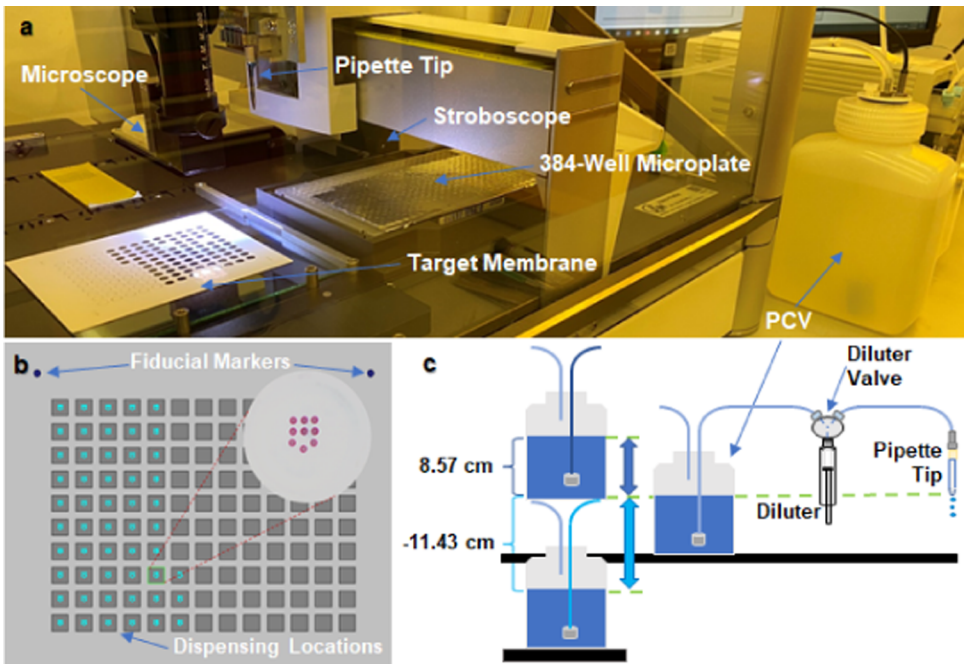

Figure 1. NP2.1 setup with a labeled work plate and desktop components required for paper-based immunoassay fabrication (a). Target membrane file from SFE software with an example of a VFI membrane disk depicting the 9-spot array pattern in colorimetric signal after performing the immunoassay (b). Block diagram of experimental setup to adjust nozzle hydrostatic pressure (c).

as the fluid viscosity, density, surface energies of fluid, and fluid/nozzle interface etc.). This prompts the use of a designed experiment to study the compounded effects of a single parameter. Furthermore, design of experiments (DOE) is a structured approach to multivariable testing that allows investigators to discover cause-and-effect relationships between multiple variables and responses of interest.[18] In contrast to changing one-factor-at-a-time (OFAT), DOE makes use of a factorial experimental strategy that changes factors together, allowing investigators to determine the effects of the individual factors and interaction effects between them, which the OFAT strategy is not capable of. These interactions are widely encountered in experiments involving chemical, biochemical, biological, electronic, and mechanical systems, and properly chosen experimental designs allow quantitative modeling between main effects, interactions, and polynomial effects of important design factors and the responses of interest.

Based on the rationale mentioned above, this paper describes the optimization of DOD piezoelectric printing of cAb arrays on NC membranes for vertical flow immunoassay (VFI) diagnostics of biothreat infectious disease biomarker YpF1 (F1 antigen of Y. pestis) using DOE. To accomplish this, a GeSiM Nano-Plotter system (NP2.1) was used. The effects of cAb concentration and nozzle hydrostatic pressure on the (i) printability of a condition, defined by the number of NC membrane disks that can be printed in a single print; (ii) jet straightness captured by the stroboscopic imaging; and (iii) cAb microarray quality represented by the misalignment of the printed array and elongation of the spot were studied. The optimized process improved printability from the initial 10 VFI membrane disks per print to the final 130 in a single print. The microarray quality of the printed 130 membrane disks was analyzed by both real VFI performance and protein staining. After these analyses, it was determined that the first 50 membrane disks of such a print had higher microarray quality and would be better suited for VFI. The DOE approach and our results could offer more insight into the antibody microarray printing process to support the efforts of others in the field.

2. MATERIALS AND METHODS

2.1. Materials. An NP2.1 piezoelectric system was purchased from GeSiM, Germany, with an Airwin BO-CT1 humidifier from BOGA, Germany. A CO_2 laser cutter (Versalaser 2.3) was purchased from Universal Laser Systems, AZ. Nitrocellulose (NC) membrane sheets of 0.45 μm pore size and 9 cm × 8 cm size were obtained from Cytiva Life Sciences, MA. Polyethersulfone (PES) syringe filters of pore size 0.2 μm were obtained from GE Healthcare. Holders for the NC membrane sheets were CNC-machined (MDX-540, Roland) in house at the Center for Applied NanoBioscience and Medicine, University of Arizona—College of Medicine, Phoenix. Yp11C7 (11C7) cAb, YpF1 antigen (F1), and gold nanoparticle-labeled Yp3F2 (AuNP-3F2) detection antibody (dAb) were produced in house by the AuCoin Laboratory at the University of Nevada, Reno. Goat anti-mouse IgM + IgA + IgG control antibody reagent was purchased from Southern Biotech, Birmingham, Al. Ponceau S staining solution, PBS, sodium phosphate monobasic and dibasic, and BSA were obtained from Sigma-Aldrich. Triton X-100 was obtained from Promega. An optical imager CanoScan 9000F Mark II was obtained from Canon. Syringe pumps were obtained from New Era Pump Systems, Inc. Luer-Lock syringes of 5 mL capacity were obtained from Becton, Dickinson and Company.

2.2. Material Preparation. NC membrane sheets (9 cm × 8 cm) were prepared into target membranes on a bench top CO_2 laser cutter at 1% power, 100% speed, and 3 mm depth. These target membranes have circular disks (3.5 mm diameter) cut into them in a 10 × 13 design with fiducial markers for targeting the cAb dispensing locations during microarray printing (Figure 1a,b). Target membranes were stored in a plastic holder and sealed with parafilm until use.

https://doi.org/10.1021/acsomega.2c03595
ACS Omega 2022, 7, 32262−32271

11C7 cAb was diluted to working concentrations (1.5, 2.5, and 5 mg/mL) using filtered 1× PBS. Control antibody reagent was prepared to a 0.5 mg/mL working concentration.

2.3. Equipment Setup. In a clean room environment, a Nano-Plotter NP2.1 was used for noncontact piezoelectric microarray printing of cAbs onto circular disks of the target membrane as shown in Figure 1a. To prevent evaporation of reagents during printing, an ambient humidity of 55% was maintained using a humidifier. The nozzle hydrostatic pressure was controlled during the experiment by either raising (8.57 cm) or lowering (−11.43 cm) the pressure compensation vessel (PCV) from the pipette tip height (Figure 1c). Spot-Front-End (SFE) software was utilized to coordinate a spotting plan for use in the Nano-Plotter control software (NPC16), beginning with creating a 9-spot pattern of the antibody microarray. In the SFE software, this spot pattern was then selected at the first 50 dispensing locations on a target membrane file. A representation of the target membrane file is shown in Figure 1b. A 384-well microplate (4309849, Applied Biosystems) was used to aspirate the antibodies for dispensing. 11C7 was dispensed in 20, 40, or 50 droplets per spot for 5, 2.5, and 1.5 mg/mL solutions, respectively, to saturate the NC membrane at the top 2 rows (6 spots) of the 9-spot pattern. Twenty droplets of goat anti-mouse control reagent were dispensed at the bottom 3 spots of the 9-spot pattern.

2.4. Antibody Microarray Fabrication. The PCV was set to the specified height, and the droplet angle failure was checked with deionized (DI) water using the stroboscope test feature to ensure successful dispensing of droplets before running each print. Test and control reagents were then vortexed and pipetted into wells of a 384-well microplate corresponding to the locations specified in the transfer steps of the spotting plan. Target membranes were loaded onto a glass substrate and placed on the work plate. The fiducial marks of the target membrane were visualized under a microscope and specified in the software to determine where to execute the spotting plan (Figure 1a). The SFE program in run mode of NPC16 was utilized for spotting plan execution, and an advanced wash parameter was input to clean the pipette tip by aspirating 0.2 M NaOH and performing additional flushing with DI water before, during, and after microarray printing to clean the pipette interior and decontaminate for subsequent samples.

2.5. Experimental Design. To design the characterization/optimization experiment, cAb concentration and PCV height were included as factors in the designed experiment. Since both factors are quantitative and optimization is the objective, a reasonable choice of statistical model for the experiment is a second-order polynomial. The Custom Design platform in the JMP Pro V16 software (JMP, Version 16. SAS Institute Inc., Cary, NC, 1989−2021) and the D-optimal criterion were used to construct the design. This design was constructed, and the optimality criteria was employed according to previous literature.[19,20] Three levels of each factor were tested in the experiment: cAb concentrations at 1.5, 2.5, and 5 mg/mL and PCV heights at −11.43, 0, and 8.57 cm. It was decided that 9 runs per day was feasible so a 3^2 factorial design worked well. The 9-run design produced by the software was approximately 44% D-efficient and approximately 75% G-efficient. Since the design would be used both to measure the effects of the individual factors and for prediction, these design performance measures are reasonable. There was some correlation between the linear and quadratic terms that resulted for the nonorthogonal structure of the design, but this varied between approximately 0.05 and 0.24, and was not considered problematic. Because a moderately large amount of random error in the system was anticipated, replicating the original 9-run design was necessary. Three replicates were decided to be adequate, with each replicate completed within a day. The experimental strategy enabled the treatment of replicates as blocks in the statistical analysis so that variability over time (days) could be eliminated from the results. This resulted in the 27-run design shown in Table S1 of the Supporting Information. The runs in Table S1 are shown in a standard order; the actual run order on each day was randomized and is shown in Table 1.

Table 1. Summary of the Factor Patterns in the Order of Occurrence[a]

factor pattern	cAb concentration (mg/mL)	PCV height (cm)
33	5	8.57
11	1.5	−11.43
31	5	−11.43
22	2.5	0
21	2.5	−11.43
13	1.5	8.57
23	2.5	8.57
32	5	0
12	1.5	0

[a]Factor patterns are the combination of levels (1−3) for each input factor.

2.6. Recording Printing Responses. After printing, the membrane disks were dipped into a Ponceau stain to visualize the spotted cAb. The printability response was determined by staining these membranes backward from the 50th disc to identify the location where cAb dispensing first failed.

Besides printability, stained membrane disks were assessed for antibody microarray quality, i.e., printing misalignment and spot elongation, by analyzing with ImageJ.[21] The printing misalignment can be calculated as

$$\text{misalignment} = \sqrt{\Delta_{lateral}{}^2 + \Delta_{vertical}{}^2} \quad (1)$$

where $\Delta_{lateral}$ and $\Delta_{vertical}$ are the lateral and vertical misalignment, respectively, as shown in Figure 2a. The values of $\Delta_{lateral}$ and $\Delta_{vertical}$ were calculated using the following equations:

$$\Delta_{lateral} = \sin\theta \times D \quad (2)$$

$$\Delta_{vertical} = \sqrt{D^2 - \Delta_{lateral}{}^2} - 400\ \mu\text{m} \quad (3)$$

where D is the distance between the adjacent control and test spots, θ is the angle shift of the test spot from the control spot, and 400 μm is the standard array period (Figure 2b).

To measure the spot elongation, the long and short diameters were measured for each test spot using the line tool in the dropdown menu of the software controller. Long diameters were divided by the short diameters and averaged to give the average spot elongation for each printed membrane disc.

For the angle of failure analysis, stroboscope images that reported the angle of failure measurement for each print were saved into labeled folders and a stroboscope score (S score) was determined for each image by giving a value of 0 for no

https://doi.org/10.1021/acsomega.2c03595
ACS Omega 2022, 7, 32262−32271

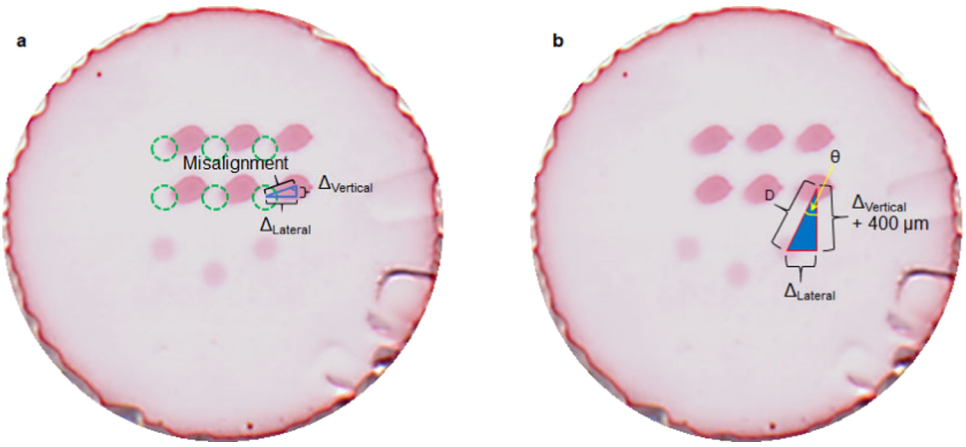

Figure 2. Example of a stained membrane disc with a right triangle depicting the misalignment between the actual test spot placement and the ideal spot location (green circles) (a). A right triangle is shown depicting the measured distance (D) and angle (θ) used to determine $\Delta_{lateral}$ and $\Delta_{vertical}$ (b).

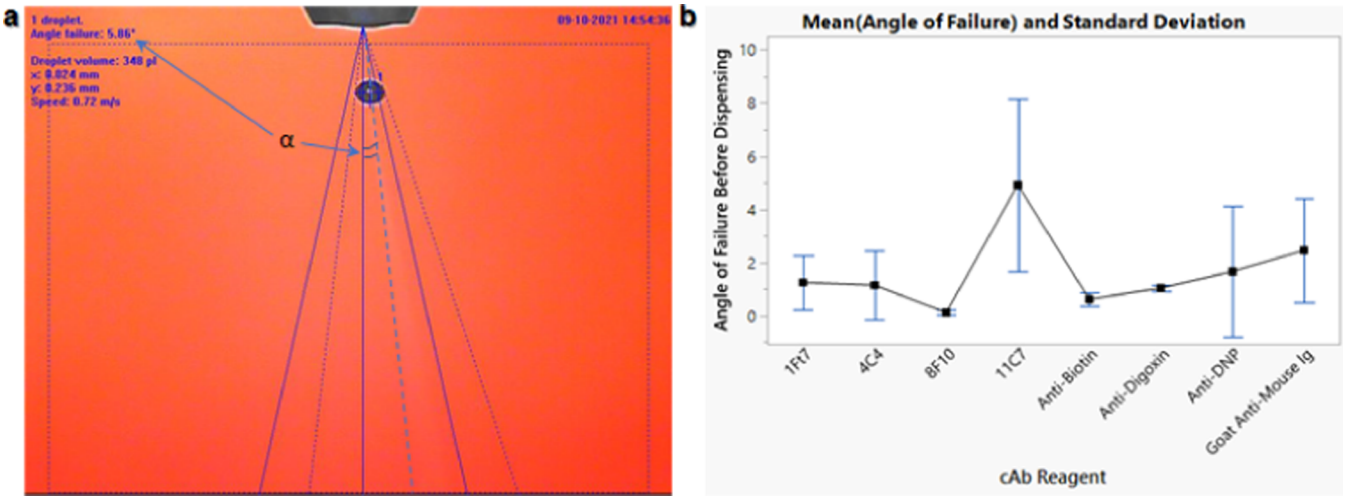

Figure 3. Example of a stroboscope check image captured when dispensing with 2.5 mg/mL 11C7 and the angle of failure measurement denoted by α (a). Angle of failure measurements taken during stroboscope checks before dispensing were averaged for various cAbs (b).

droplet, 1 for a droplet outside of the passing range (angle of failure measurement > 11°), or 2 for a droplet within the passing range. The S scores were summated for each run and subject to further analysis along with the printability and misalignment responses.

2.7. Immunochromatography Assay in VFI Devices. Assay buffer (0.1 M phosphate buffer containing 0.1% Triton X-100 and 0.5% BSA, pH 7.2) was spiked with recombinant F1 protein to a final concentration of 5 and 1 ng/mL. AuNP-3F2 dAb (OD 20) was added to the solution and incubated for 10 min on a rocker. The 5 mL samples were then filtered with 0.2 μm PES syringe filters and loaded into 5 mL Luer-Lock syringes. Samples were flown through a custom-built VFI device at 0.2 mL/min and dried for 10 min before scanning. After drying, the VFI membrane disks were scanned with a flatbed optical scanner (CanoScan 9000 FII) to measure the signal intensity of the test spots as described in previous literature.[1]

3. RESULTS

3.1. Analysis of Different cAbs. It was observed that different cAbs displayed varied success in microarray printing at concentrations ranging from 0.1 to 10 mg/mL. To begin investigating this, stroboscope images were examined from a compilation of different antibody microarray printings. From these stroboscope images, the angle of failure for printing was measured according to droplet deviation from the median line (Figure 3a). The angle of failure measurement before dispensing was proposed to be negatively associated with the success of a print for each cAb. For this study, the cAb with the highest average and largest variability in angle of failure measurement was selected (Figure 3b). After selecting 11C7, an attempt to increase cAb concentration beyond the 2.5 mg/mL threshold was tested to see whether it would improve microarray printing. Through trial efforts, the possibility of a receding meniscus when printing at high cAb concentrations was brought to attention from the device manufacturers, along with suggestion to attempt increasing nozzle hydrostatic pressure. Thus, to optimize this antibody microarray printing process, the two input variables cAb concentration and nozzle hydrostatic pressure were chosen.

3.2. Exploratory Data Analysis. To investigate the effect of hydrostatic pressure in this designed experiment, 11C7 was aspirated and dispensed under a stroboscope camera while the height of the PCV was adjusted. It was found that raising the PCV 11.43 cm caused no droplet formation due to liquid

https://doi.org/10.1021/acsomega.2c03595
ACS Omega 2022, 7, 32262−32271

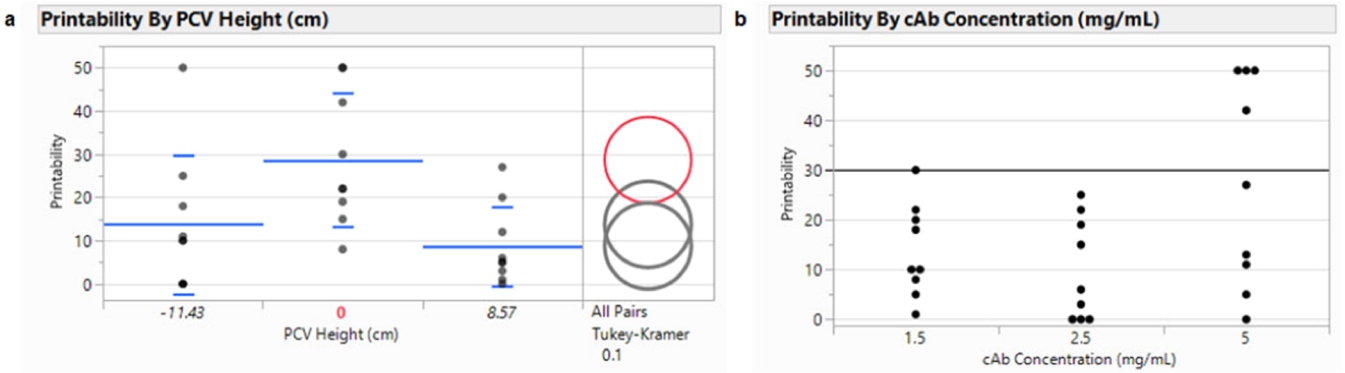

Figure 4. Number of membrane disks printed by PCV height from the level of the pipette tip, with horizontal blue lines representing the means and standard deviations for each group of data points (a). The comparison circles represent the group mean comparisons using the Tukey−Kramer HSD (honestly significant difference) test with $\alpha = 0.1$. Number of membrane disks printed by cAb concentration (b).

Table 2. Summary of Term Effect on Printing Responses

effect estimate summary		
term	printability	S score
intercept	22.58[a]	3.38[a]
cAb concentration (mg/mL)	4.14	−0.11
PCV height (cm)	−4.23	−0.09
cAb concentration (mg/mL) × PCV height (cm)	0.14	0.10
cAb concentration (mg/mL) × cAb concentration (mg/mL)	9.41	0.58
PCV height (cm) × PCV height (cm)	−18.12[a]	−1.52[a]
block (day 1)	−0.07	−0.44
block (day 2)	−4.63	0.11
block (day 3)	4.70	0.33

[a]Coefficient estimates with corresponding *p*-values below 0.05.

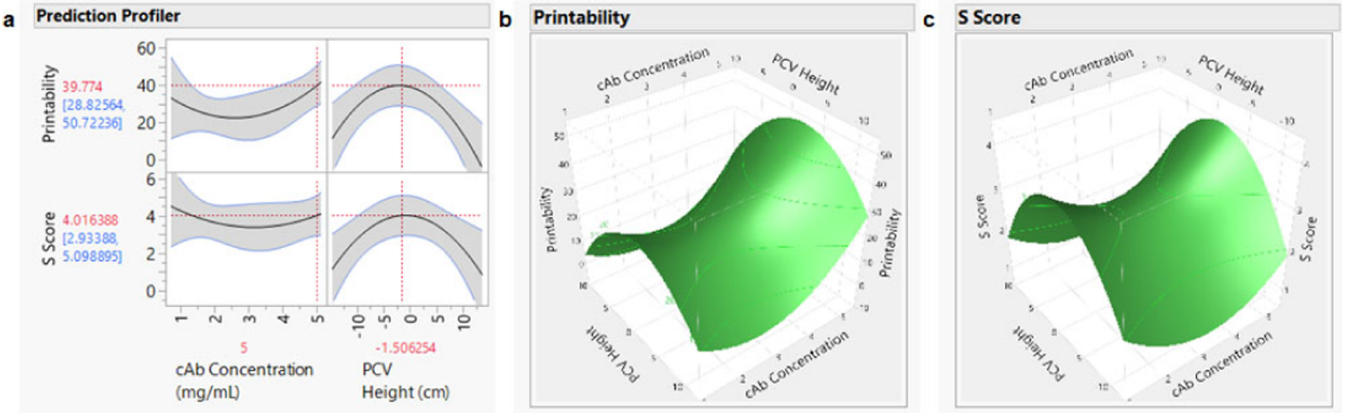

Figure 5. Printability and S score printing response values were analyzed with the Fit Model platform in JMP and a prediction profiler was produced to reflect the program's expected outcomes for each variable input (a). The variable inputs that predicted the best outcome are highlighted in red. Printability (b) and S score (c) response values were graphically represented as a function of cAb concentration and PCV height in the response surfaces.

accumulation; however, lowering the PCV within the range of its tubing did not prevent droplet formation. Thus, 75% of both the raised height (8.57 cm) that caused liquid accumulation and the maximum lowered height (−11.43 cm) were selected to study the PCV height effect with continued dispensing. Exploratory data analysis revealed that the PCV height has a significant impact on printability. Printability is plotted against the PCV heights tested in Figure 4a. The Tukey HSD tests for all differences among the means and shows that the average printability for the PCV height at the level of the pipette tip is significantly different from the other two heights tested. The largest difference is between the raised and pipette tip level PCV heights. The pipette tip level PCV height produces on average 20 membrane disks more than the raised height with corresponding *p*-value = 0.015 (Table S2).

The results also show that a higher cAb concentration may yield an increase of printability. The 5 mg/mL concentration was the only level to produce a number of membrane disks greater than 30 and had 3 data points that resulted in 50 membrane disks (Figure 4b). These findings are reassuring because at higher concentrations a lower volume is needed to

https://doi.org/10.1021/acsomega.2c03595
ACS Omega 2022, 7, 32262−32271

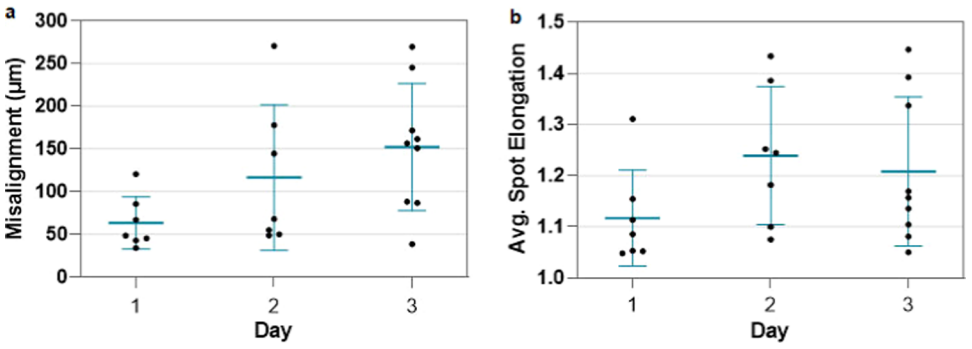

Figure 6. Printing misalignment (a) and average spot elongation (b) were reported as the misalignment between actual and ideal test spot location and elongation measurements by run order for each day. The blue lines represent the mean and standard deviation of each day.

saturate NC membranes, up to the adsorption capacity of the substrate.[22] This benefits the printing process because there is a limitation of 300 spots that can be dispensed by the nanoplotter in a given line; however, this limitation of spots can vary by the number of droplets per spot. Therefore, a reduction of droplets with the higher concentration cAb is favorable. Indeed, other groups have also recommended the printing of antibodies at the upper end of printer capacity.[12] However, this increased cAb concentration also increases the potential for clogging of the pipette tip. To address this problem, the cleaning procedures chosen to prevent the buildup of protein aggregates and precipitate comprised brief 0.2 M NaOH incubations within printing runs and an end of day incubation in a protease detergent (4% Tergazyme) for 30 min. These were followed by ∼2 mL flushing and 3 min washing cycles of the tip, respectively. The protease detergent digests proteins well; however, the long incubation time makes it unsuitable for use within printing runs. Thus, denaturing proteins with NaOH was selected for within run cleaning. Together, these procedures permit the continued aspiration and dispensing of cAbs up to 5 mg/mL with the Nano-Tip A-R-J pipette head (GeSiM, GmbH). The quality of this dispensing was assessed by the S score which was determined from stroboscopic imaging within printing runs.

3.3. Analysis of the Designed Experiment. The printability and S score printing responses were analyzed using the Fit Model platform in JMP Pro V16 to test significance of model effects and to find the predictability of these results. The effect estimate summary is listed in Table 2 and includes the estimates of the coefficients in the full quadratic model for each response. The quadratic term for the PCV height was statistically significant for both responses, printability and S score. This relationship is represented graphically by the curvature seen in the prediction profiler of Figure 5a.

Although it was suggested that adjusting nozzle hydrostatic pressure might help with dispensing higher concentration cAb, neither increasing nor decreasing hydrostatic pressure significantly affected printability at the higher concentration level. This relationship defines the interaction term in the model, which was statistically insignificant. The designed experiment optimized printing conditions for the 11C7 reagent in a predictive fashion, and the critical parameters are given in Table 2. The most important factor that emerged in the printability response was the quadratic term for the PCV height. Figure 5a shows the prediction profiler from JMP for this response with the levels that result in the maximum response represented by the vertical dotted lines. The horizontal dotted line is the predicted value of the response at the current factor settings. Notice that the maximum printability occurs with the high level of cAb concentration and the PCV height nearest the middle level. In Figure 5b, the response surface for printability is shown, depicting a saddle point system. It is apparent here that the maximum response occurs at the high level of cAb concentration. The response rapidly drops off as the PCV height changes from the middle level.

Figure 5c includes similar plots for the S score response. Once again, the quadratic effect for the PCV height is significant in characterizing the response. The maximum value of the S score also occurs when cAb concentration is at the high level and the PCV height is nearest the middle level. This response surface in Figure 5c is a saddle point, and it is clear that the response decreases rapidly as the PCV height changes from the middle level. This sharp drop-off effect may be due, in part, to a few reasons. To analyze the results for all stroboscope checks, we had to create a value-based system to account for instances where no droplet was found in frame and no subsequent angle could be recorded. Such instances occurred due to an inability for a droplet to be ejected from, or when liquid accumulated at, the tip of the pipette. Both of these scenarios resulted more often when nozzle hydrostatic pressure was increased or decreased due to raising or lowering the PCV height. If droplet formation failed before printing, then no membrane disks would be printed and a total S score of 0 was given. If it occurred only after printing, then it was likely following premature discontinuation of dispensing and a total S score of 1 or 2 was given. Therefore, proper nozzle hydrostatic pressure is important for higher printability. The results of the analysis in JMP support the observed optimal parameters from the designed experiment, with the highest printability being achieved with 5 mg/mL of cAb and PCV nearest the pipette tip height. Due to the flatness of the PCV height curve in the prediction profilers for printability and S score, the middle PCV height was selected for the purpose of simplicity in further study.

The observed agreement between printability and S score is reasonable because our criteria for a higher score was a droplet within passing range (angle of failure measurement < 11°), as captured by stroboscopic imaging. Therefore, a higher printability may be more likely to result if a droplet is present and its trajectory is tolerable in the stroboscope check. Both S score and printability increased when the PCV remained at the pipette tip height, where nozzle hydrostatic pressure is closest to equilibrium. Nozzle hydrostatic pressure is important for optimized microarray printing and is further influenced by

https://doi.org/10.1021/acsomega.2c03595
ACS Omega 2022, 7, 32262−32271

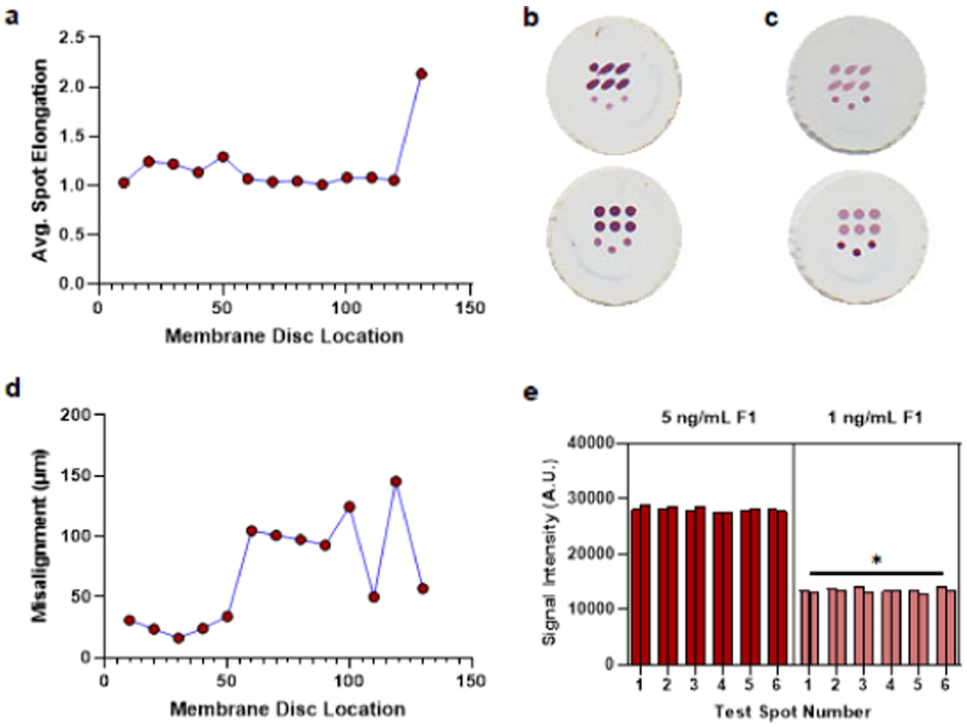

Figure 7. Spot elongation (a) and printing misalignment (d) were reported for every 10th membrane disc location. Scanned images of 9-spot colorimetric signals after performing the assay with the 1st and 130th (b), and 2nd and 129th (c) membrane disks, respectively. Signal intensities of all 6 test spots were compared between the 1st and 130th, and 2nd and 129th membrane disks, when run with 5 and 1 ng/mL of F1 antigen in buffer, respectively (e). Student's paired t test $p = 0.0219$.

maintenance procedures. These procedures for preventive maintenance (PM) include the replacing of particle filters every 6 months and running of filtered 70% ethanol through the PCV filter and subsequent tubing every couple of months. We have found improvement with microarray printing following these PMs, suggesting their beneficial impact on the system's nozzle hydrostatic pressure. Therefore, a PM was performed immediately before beginning the first replicate of the designed experiment.

3.4. Analysis of Antibody Microarrays. To investigate antibody microarray quality after printing, the printing misalignment and spot elongation were reported quantitatively by run order for each day. In Figure 6a, we see that mean misalignment increases with each subsequent day. This may suggest that misalignment increases as more prints are run and more time has elapsed since the preventive maintenance was last done. Additionally, Figure 6b shows that the mean of average spot elongation was lowest on the first day and remained similarly elevated for the subsequent days. It is also worth noting that printing conditions that resulted in a printability of zero did not have membrane disks to quantitatively assess.

3.5. Analysis of Optimized Printing. To characterize the overall impact of the optimized parameters for printing 11C7 a decision was made to execute a print targeting all 130 dispensing locations on the target membrane. Before this was done, the system's filter in the PCV and subsequent tubing was cleaned as mentioned previously. It was found that all membrane disc locations were successfully printed, and every 10th membrane disc of this batch was quantitatively assessed for antibody microarray quality (Figure 7). The average test spot elongation remained fairly circular over the course of the print, before elongating over the last 10 membrane disc locations (Figure 7a). This occurred due to the effect where the test spots begin to streak toward the upper right of the membrane disc (Figure 7b,c). This effect increases the overall spot elongation measurement.

In Figure 7d, misalignment between ideal and actual test spot location remains lower than a 50 μm pitch for the first 50 membrane disc locations, doubles for the next 40, and then becomes inconsistent over the last 40 locations. Taken together, we can see that antibody microarray quality remains most consistent and precise over the first 50 membrane disc locations, but then misalignment begins to suffer, and the spots lose circularity over the last 10 locations. The change in spot shape may decrease cAb density and therefore impact signal intensity. This prompted investigation into whether immunoassay performance would be impacted.

As shown in Figure 7e, there was no statistical significance in mean differences between the signal intensities of the first and last membrane disks when ran with 5 ng/mL of F1 antigen in buffer (Figure 7b). However, the next membrane disks in order (Figure 7c) did show statistical significance between mean differences in signal intensity when ran with 1 ng/mL of F1, though the difference in mean values was relatively small (−517.9 AU). These results may suggest that assay sensitivity decreases for membrane disks at the end of this size of print. Altogether, these results demonstrate an improvement in printability from our previous successes printing antibody microarrays with 2.5 mg/mL of 11C7 onto NC membrane disks, where the average batch size was 8−10. Additionally, these results set a benchmark for determining a production size with tolerable intrabatch variability.

https://doi.org/10.1021/acsomega.2c03595
ACS Omega 2022, 7, 32262−32271

4. DISCUSSION

A traditional DOE study starts with a screening study to identify critical parameters, then is followed by additional designed experiments focused on optimization of the variables identified as important. In this study, some parameters have been tested beforehand. For example, the electrical pulse voltage and width for DOD piezoelectric inkjet printing were found to be optimal at 90 V and 50 μs for all cAb printed. There were also other prestudies before the DOE. For example, different cAbs were tested and the worst performing one was selected for the DOE. Additionally, it is important to saturate the NC membrane with adsorbed cAb for VFI assay, so the number of droplets per spot to saturate the NC membrane was identified for each cAb concentration. With these studies to set constraints and eliminate some variables, our current study focused on the two most likely variables to impact the printing process as suggested by the manufacturer, i.e., PCV height and cAb concentration, for the DOE study.

It is also important to understand the underlying physical mechanisms of the experimental results to further improve the printing process. The designed experiment identified the PCV at the pipette tip height and the highest cAb concentration (5 mg/mL) as the optimal conditions for printing. The role of PCV height is to provide the right hydrostatic pressure (P_h) at the micropipette orifice and, together with the capillary pressure (P_c) at the orifice, to avoid either liquid accumulation at the tip or a withdrawing meniscus inside the tip, which could both prevent droplet formation. To understand the interaction between P_h and P_c, the cAb solution contact angles on both silicon and glass (the materials of the micropipette, Figure S1) were measured to be ~20°, i.e., wetting the micropipette surfaces. Based on previous analysis of liquid bursting out an orifice,[23] the required pressure to let the fluid flow out of the 50 μm sized orifice would be ~1.9 kPa (Supporting Information Figure S1b and eq S1c). On the other hand, P_h from the 8.57 cm height increase of the PCV is 0.86 kPa (Supporting Information eq S1a), which is on the same order with the 1.9 kPa P_c but slightly lower. This is consistent with our observation that the 8.57 cm PCV height did not cause a quick liquid accumulation at the tip to prevent droplet formation. However, our results also indicate that this increased height may still cause some liquid accumulation gradually over the repeated droplet jetting process.

When the PCV is lowered to 11.43 cm, there is a P_h of ~−1.16 kPa (Supporting Information eq S1a) to withdraw the liquid away from the orifice. The P_c from the meniscus can be calculated to be ~5.15 kPa (Supporting Information eq S1d), which is large enough to keep the liquid at the orifice. However, after jetting out a droplet, the fluid needs to be replenished and the negative P_h could slow down the process which may prevent further droplet formation, especially over fast repeated droplet jetting. Overall, the above analysis explained qualitatively that the optimal PCV height was found to be with its water level around that of the pipette tip height for our current micropipette surface condition and the corresponding cAb solution contact angle.

To understand the effect of cAb concentration, it is complicated when considering the effects of fluid density, viscosity, surface tension etc. analytically for cAb solutions with different concentrations. However, our experiments have indicated a trend that printing tends to get worse with repeated droplet jetting. Since higher concentration cAb requires less droplets per spot to saturate the NC membrane, it is reasonable to expect that the 5 mg/mL cAb solution that required the least amount of droplet jetting performed the best.

5. CONCLUSIONS

In the present study, we utilized a statistically designed experiment to optimize a process for printing antibody microarrays with noncontact piezoelectric dispensing, which is advantageous for the described application compared to others due to its high-capacity printing, easily adjustable droplet control, and a lowered risk of damaging sensitive solutions and substrates. The randomization and factorial design structure of the experiment allowed for more robust and quantitative reporting of the main effects and their interactions in this printing process. A 5 mg/mL concentration of 11C7 was successfully printed and yielded an increase in printability compared to the previously utilized cAb concentration of 2.5 mg/mL. Additionally, an increase in hydrostatic pressure was not needed to print at this higher cAb concentration as printability decreased significantly when the PCV was raised from the pipette tip height. The optimal printing condition at 5 mg/mL cAb concentration and zero PCV height showed a 13-fold improvement in the printability (from 10 to 130 membrane disks per printing). The first 50 membrane disks of this print size showed greater potential for reliable use in immunoassay. The daily misalignment data also suggested that our maintenance procedures played a role in the process.

In the future, additional maintenance procedures will be tested to improve the array location accuracy. Micropipette surfaces with different cAb contact angles could be explored for improved printing as well. We will also use this optimized process to print additional cAbs to fabricate multiplexed VFI membrane disks and plan to further scale production with a longitudinal stability study of antibody microarray performance.

■ ASSOCIATED CONTENT

Supporting Information

The Supporting Information is available free of charge at https://pubs.acs.org/doi/10.1021/acsomega.2c03595.

Additional experimental design details, response values from DOE analyses, *p*-values from exploratory data analysis, and hydrostatic and capillary pressure calculation (PDF)

■ AUTHOR INFORMATION

Corresponding Authors

Alexander J. Summers − *Center for Applied NanoBioscience and Medicine, College of Medicine, University of Arizona, Phoenix, Arizona 85004, United States;* orcid.org/0000-0002-7372-0610; Email: ajsummers@arizona.edu

Jian Gu − *Center for Applied NanoBioscience and Medicine, College of Medicine, University of Arizona, Phoenix, Arizona 85004, United States; Department of Basic Medical Sciences, The University of Arizona, College of Medicine, Phoenix, Arizona 85004, United States;* Email: jgu10@arizona.edu

Douglas C. Montgomery − *School of Computing and Augmented Intelligence, Arizona State University, Tempe, Arizona 85287-1004, United States;* Email: doug.montgomery@asu.edu

https://doi.org/10.1021/acsomega.2c03595
ACS Omega 2022, 7, 32262−32271

Frederic Zenhausern − *Center for Applied NanoBioscience and Medicine, College of Medicine, University of Arizona, Phoenix, Arizona 85004, United States; Department of Basic Medical Sciences, The University of Arizona, College of Medicine, Phoenix, Arizona 85004, United States; Department of Biomedical Engineering, The University of Arizona, College of Engineering, Tucson, Arizona 85721, United States*; Email: fzenhaus@arizona.edu

Authors

Jasmine P. Devadhasan − *Center for Applied NanoBioscience and Medicine, College of Medicine, University of Arizona, Phoenix, Arizona 85004, United States*

Brittany Fischer − *School of Computing and Augmented Intelligence, Arizona State University, Tempe, Arizona 85287-1004, United States*

Marcellene A. Gates-Hollingsworth − *Department of Microbiology and Immunology, University of Nevada School of Medicine, Reno, Nevada 89557-0705, United States*

Kathryn J. Pflughoeft − *Department of Microbiology and Immunology, University of Nevada School of Medicine, Reno, Nevada 89557-0705, United States*

Tuan Vo-Dinh − *Fitzpatrick Institute for Photonics, Departments of Biomedical Engineering and Chemistry, Duke University, Durham, North Carolina 27708-0281, United States*; orcid.org/0000-0003-3701-3326

David P. AuCoin − *Department of Microbiology and Immunology, University of Nevada School of Medicine, Reno, Nevada 89557-0705, United States*

Complete contact information is available at: https://pubs.acs.org/10.1021/acsomega.2c03595

Author Contributions

Conceptualization: A.J.S., J.P.D., J.G., D.C.M., B.F., and F.Z.; methodology: A.J.S., J.P.D., J.G., D.C.M., and B.F.; formal analysis: A.J.S., D.C.M., and B.F.; investigation: A.J.S.; data curation: A.J.S., D.C.M., and B.F.; writing—original draft preparation: A.J.S.; writing, review, and editing: J.P.D., J.G., D.C.M., B.F., M.A.G., K.J.P., D.P.A., T.V., and F.Z.; supervision: J.P.D., J.G., D.C.M., and F.Z. All authors have given approval to the final version of the manuscript.

Funding

This work was supported by the Chemical Biological Technologies Directorate [Contract # HDTRA1-16-C-0026] and the Advanced Technology International [Contract # MCDC-18-04-09-002] from the Department of Defense Chemical and Biological Defense program through the Defense Threat Reduction Agency (DTRA).

Notes

The authors declare no competing financial interest.

■ ACKNOWLEDGMENTS

Special thank you to Sujata Pandit, Derrick Hau, Ali Fattahi, and Supriya Atta for their expertize and contribution to our study and assistance in writing the manuscript. This work was supported by the Chemical Biological Technologies Directorate [Contract # HDTRA1-16-C-0026] and the Advanced Technology International [Contract # MCDC-18-04-09-002] from the Department of Defense Chemical and Biological Defense program through the Defense Threat Reduction Agency (DTRA).

■ NOMENCLATURE

NC, nitrocellulose; cAb, capture antibody reagent; AFM, atomic force microscopy; CIJ, continuous inkjet; DOD, drop on demand; DOE, design of experiment; OFAT, one-factor-at-a-time; VFI, vertical flow immunoassay; NP2.1, nano-plotter system; PES, polyethersulfone; 11C7, Yp11C7; F1, YpF1; AuNP-3F2, gold nanoparticle-labeled Yp3F2; dAb, detection antibody; PCV, pressure compensation vessel; SFE, spot-front-end; NPC16, nano-plotter controller software; DI, deionized; S score, stroboscope score; PM, preventive maintenance; P_h, hydrostatic pressure; P_c, capillary pressure

■ REFERENCES

(1) Devadhasan, J. P.; Gu, J.; Chen, P.; Smith, S.; Thomas, B.; Gates-Hollingsworth, M.; et al. Critical Comparison between Large and Mini Vertical Flow Immunoassay Platforms for Yersinia Pestis Detection. *Anal. Chem.* **2021**, *93*, 9337−9344.

(2) Chinnasamy, T.; Segerink, L. I.; Nystrand, M.; Gantelius, J.; Svahn, H. A. Point-of-care vertical flow allergen microarray assay: Proof of concept. *Clin. Chem.* **2014**, *60*, 1209−1216.

(3) Kumar, S.; Nehra, M.; Khurana, S.; Dilbaghi, N.; Kumar, V.; Kaushik, A.; Kim, K. H. Aspects of point-of-care diagnostics for personalized health wellness. *Int. J. Nanomed.* **2021**, *16*, 383−402.

(4) Ross, G. M. S.; Salentijn, G. I.; Nielen, M. W. F. A critical comparison between flow-through and lateral flow immunoassay formats for visual and smartphone-based multiplex allergen detection. *Biosensors* **2019**, *9*, No. 143.

(5) Cretich, M.; Torrisi, M.; Daminelli, S.; Gagni, P.; Plavisch, L.; Chiari, M. Flow-through, viral co-infection assay for resource-limited settings. *Talanta* **2015**, *132*, 315−320.

(6) Chen, P.; Gates-Hollingsworth, M.; Pandit, S.; Park, A.; Montgomery, D.; AuCoin, D. P.; et al. Paper-based Vertical Flow Immunoassay (VFI) for detection of bio-threat pathogens. *Talanta* **2019**, *191*, 81−88.

(7) Joung, H-A.; Ballard, Z. S.; Ma, A.; Tseng, D. K.; Teshome, H.; Burakowski, S.; et al. Paper-based multiplexed vertical flow assay for point-of-care testing. *Lab Chip* **2019**, *19*, 1027−1034.

(8) Romanov, V.; Brooks, B. D. Antibody Printing Technologies. *Methods Mol. Biol.* **2021**, *2237*, 151−177.

(9) Sun, Y.-S. Use of Microarrays as a High-Throughput Platform for Label-Free Biosensing. *SLAS Technol.* **2015**, *20*, 334−353.

(10) Gupta, S.; Manubhai, K. P.; Kulkarni, V.; Srivastava, S. An overview of innovations and industrial solutions in Protein Microarray Technology. *Proteomics* **2016**, *16*, 1297−1308.

(11) Kahng, S.-J.; Cerwyn, C.; Dincau, B. M.; Kim, J-H.; Novosselov, I. V.; Anantram, M. P.; Chung, J.-H. Nanoink bridge-induced capillary pen printing for chemical sensors. *Nanotechnology* **2018**, *29*, No. 335304.

(12) Pilobello, K. T.; Agrawal, P.; Rouse, R.; Mahal, L. K. Advances in lectin microarray technology: Optimized protocols for piezoelectric print conditions. *Curr. Protoc. Chem. Biol.* **2013**, *5*, 1−23.

(13) Sarkar, J.; Kumar, A. Recent Advances in Biomaterial-Based High-Throughput Platforms. *Biotechnol. J.* **2021**, *16*, No. 2000288.

(14) Ru, C.; Luo, J.; Xie, S.; Sun, Y. A review of non-contact micro- and nano-printing technologies. *J. Micromech. Microeng.* **2014**, *24*, No. 053001.

(15) Derby, B. Inkjet printing of functional and structural materials: Fluid property requirements, feature stability, and resolution. *Annu. Rev. Mater. Res.* **2010**, *40*, 395−414.

(16) Romanov, V.; Davidoff, S. N.; Miles, A. R.; Grainger, D. W.; Gale, B. K.; Brooks, B. D. A critical comparison of protein microarray fabrication technologies. *Analyst* **2014**, *139*, 1303−1326.

(17) Wijshoff, H. The dynamics of the piezo inkjet printhead operation. *Phys. Rep.* **2010**, *491*, 77−177.

(18) Uy, M.; Telford, J. K.Optimization by Design of Experiment Techniques. In *IEEE Aerospace Conference Proceedings*; IEEE, 2009, DOI: 10.1109/AERO.2009.4839625.

(19) Jones, B.; Montgomery, D. C. *Design of Experiments: A Modern Approach*, 1st ed.; Wiley: Hoboken, NJ, 2019; pp 118−203.
(20) Montgomery, D. C. *Design and Analysis of Experiments*, 10th ed.; Wiley: Hoboken, NJ,, 2019; pp 172−477.
(21) Schindelin, J.; Arganda-Carreras, I.; Frise, E.; Kaynig, V.; Longair, M.; Pietzsch, T.; et al. Fiji: An open-source platform for biological-image analysis. *Nat. Methods* **2012**, *9*, 676−682.
(22) O'Farrell, B.; Rosen, S.; Ponti, J. S.; Brown, M. C.; Chun, P.; Mansfield, M. A.et al. *Nitrocellulose Membranes for Lateral Flow Immunoassays: A Technical Treatise BT - Lateral Flow Immunoassay*; Wong, R.; Tse, H., Eds.; Humana Press: Totowa, NJ, 2009; pp 100−101, DOI: 10.1007/978-1-59745-240-3_6.
(23) Agonafer, D. D.; Lee, H.; Vasquez, P. A.; Won, Y.; Jung, K. W.; Lingamneni, S.; et al. Porous micropillar structures for retaining low surface tension liquids. *J. Colloid Interface Sci.* **2018**, *514*, 316−327.

https://doi.org/10.1021/acsomega.2c03595
ACS Omega 2022, 7, 32262−32271